Conformal Complex Singlet Extension of the Standard Model: Scenario for Dark Matter and a Second Higgs Boson

Zhi-Wei Wang and T.G. Steele
Department of Physics and Engineering Physics, University of Saskatchewan, Saskatoon, SK, S7N 5E2, Canada

T. Hanif
Department of Theoretical Physics, University of Dhaka, Dhaka-1000, Bangladesh

R.B. Mann
Department of Physics, University of Waterloo, Waterloo, ON, N2L 3G1, Canada

arXiv:1510.04321v2 [hep-ph] 26 Oct 2015

We consider a conformal complex singlet extension of the Standard Model with a Higgs portal interaction. Two different scenarios depending on whether the global $U(1)$ symmetry of the complex singlet is broken or unbroken have been studied. In the unbroken case, the decay of the complex singlet is protected by the global $U(1)$ symmetry which leads to an ideal cold dark matter candidate with approximately 100 GeV mass along with a significant proportion of thermal relic dark matter abundance. In the broken case, we generalize our method to incorporate a renormalization-scale optimization technique and are able to provide unique predictions for all the model's couplings and masses. We have found there exists a second Higgs boson with a mass of approximately 550 GeV that mixes with the known 125 GeV Higgs with a large mixing angle $\sin\theta \approx 0.47$ consistent with current experimental limits. Furthermore, the imaginary part of the complex singlet in the broken case could provide axion dark matter for a wide range of models. In addition, we have also provided criteria to determine the symmetry breaking pattern in both the Higgs and hidden sector.

The Standard Model (SM) of particle physics is incomplete since it does not provide an explanation for dark matter. Amongst the numerous ways to go beyond the SM, Higgs portal models [1, 2] are conceptually appealing because they provide a link between Higgs hunting in collider experiments and dark matter direct detection experiments [3]. Although the real singlet extension of the SM provides the simplest Higgs portal model, the complex singlet extension with global $U(1)$ symmetry yields richer phenomenological properties, such as a second Higgs particle mixed with the ordinary Higgs particle along with WIMP dark matter candidates [4–6]. The global $U(1)$ symmetry also provides a foundation for further model-building [7–9].

Versions of singlet extensions with classical conformal symmetry are particularly interesting since they may address the hierarchy and fine-tuning problems [10, 11] associated with the conventional electroweak symmetry breaking mechanism. Classical scale invariance provides a custodial symmetry for Higgs loop corrections [11, 12], and similar to dimensional transmutation in QCD, leads to natural scale hierarchies in a unification context [13] (see also Ref. [14] for a recent discussion). In these models, there exists two main interpretations for the origin of electroweak (EW) symmetry breaking that are usually associated with different ranges of the couplings. In the first, radiative symmetry breaking (i.e., the Coleman-Weinberg (CW) mechanism [15]) in the hidden (dark) sector gets communicated to the Higgs sector. This triggers EW symmetry breaking via the Higgs portal interaction [16], which normally requires a negative Higgs portal interaction (see Ref. [17] for a clear review). Alternatively, radiative symmetry breaking could occur in the SM Higgs sector first and then be communicated to the hidden sector. In this second interpretation, a reasonably large Higgs quartic coupling is usually required to balance the large top quark Yukawa coupling and a positive Higgs portal interaction is permitted [18]. Although the small coupling solution predicted by Coleman and Weinberg [15] is destabilized by top quark Yukawa contributions, it can be stabilized by a large Higgs self-coupling solution [19, 20]. Recently it has been shown that the 125 GeV Higgs mass observed at the LHC [22, 23] can be described by radiative electroweak symmetry breaking in the large Higgs self coupling regime [21].

In this work, we build upon the methods of Refs. [18, 24] to carry out a dynamical analysis of the effective potential including both the Higgs doublet and complex singlet. The couplings, scalar mass spectrum, and dark matter interpretations emerge from this dynamical analysis, allowing us to examine the above two interpretations for the origin of EW symmetry breaking. Our analysis contains two main scenarios depending on whether or not the global $U(1)$ symmetry is spontaneously broken by a vacuum expectation value of the hidden-sector complex field. In the unbroken case we find a large Higgs self-coupling perturbative regime similar to Refs. [19–21], along with a scalar dark matter candidate that provides a significant proportion of the dark matter abundance. For the broken $U(1)$ case, we extend the optimization method proposed in [25] to multiple scalar fields to accommodate the addition of a complex-singlet vacuum expectation value. Generalizing this method to incorporate radiative symmetry breaking, we find that in addition to an ordinary Higgs particle, there exists a second Higgs boson with a 554 GeV mass and a large mixing angle satisfying current

experimental bounds, whilst being within the detection region of LHC run2. Furthermore, it also leads to an axion dark matter candidate whose properties depend on detailed model building. This method has very strong predictive power, affording dynamical generation of all the parameters in the model.

The complex singlet extension of the SM has the following scalar sector [4]:

$$L = \frac{1}{2}\partial_\mu H^\dagger \partial^\mu H + \frac{1}{2}\partial_\mu S^\dagger \partial^\mu S - \lambda_2 |S|^2 H^\dagger H - \lambda_3 |S|^4 - \lambda_1 \left(H^\dagger H\right)^2 \tag{1}$$

where H is the (complex doublet) Higgs field and S is the complex singlet field, which has no interactions with other SM fields except via the Higgs portal interaction proportional to λ_2. The above Lagrangian obeys a global $U(1)$ symmetry for S. By considering this symmetry either unbroken or broken, we can divide the phenomenology into two cases: $\langle S\rangle = 0$ and $\langle S\rangle \neq 0$. For the unbroken case, the decay of the complex singlet S is protected by the $U(1)$ global symmetry, making it an ideal cold dark matter candidate. Our analysis builds upon the Gildener-Weinberg method [24] that generalizes the Coleman-Weinberg technique [15] to incorporate multiple scalar fields. Letting $H = \frac{1}{\sqrt{2}}(\phi_1 + i\phi_2, \phi_3 + i\phi_4)$, $S = \frac{1}{\sqrt{2}}(\varphi_1 + i\varphi_2)$ and defining $\phi^2 = \sum_i \phi_i^2$ and $\varphi^2 = \sum_i \varphi_i^2$, we obtain leading-logarithm expression for the effective potential [18]

$$V_{LL} = \frac{1}{4}\lambda_1\phi^4 + \frac{1}{4}\lambda_2\phi^2\varphi^2 + \frac{1}{4}\lambda_3\varphi^4 + BL + CL^2 + DL^3 + EL^4 + \dots \tag{2}$$

where $L \equiv \log\left(\frac{\phi^2+\varphi^2}{\mu^2}\right)$. The quantities B, C, D, E are the functions of $(\lambda_1, \lambda_2, \lambda_3, g_t, \phi, \varphi)$ which are dimension-4 combinations of ϕ^2 and φ^2 as required by $O(4)$ and $U(1)$ symmetry and contain leading-logarithm (LL) combinations of couplings $\left(\lambda_1^\alpha \lambda_2^\beta \lambda_3^\gamma g_t^{2\delta}\right) L^p$ where g_t is the top Yukawa coupling and $p - (\alpha + \beta + \gamma + \delta) = 1$. The coefficients B, C, D, E are determined by RG equation

$$\left(\mu\frac{\partial}{\partial\mu} + \beta_{g_t}\frac{\partial}{\partial g_t} + \sum_{i=1}^{3}\beta_i\frac{\partial}{\partial\lambda_i} + \gamma_\phi\phi\frac{\partial}{\partial\phi}\right)V_{LL} = 0 \tag{3}$$

where the RG functions β_i, β_{g_t} and anomalous dimensions γ_ϕ are given by [26]

$$\begin{aligned}
\beta_1 &= \frac{1}{16\pi^2}\left(24\lambda_1^2 + \lambda_2^2 - 6g_t^4 + 12\lambda_1 g_t^2\right)\\
\beta_2 &= \frac{1}{16\pi^2}\left(8\lambda_2\lambda_3 + 6\lambda_1\lambda_2 + 16\lambda_2^2 + 6\lambda_2 g_t^2\right)\\
\beta_3 &= \frac{1}{16\pi^2}\left(\frac{1}{2}\lambda_2^2 + 20\lambda_3^2\right)\\
\beta_{g_t} &= \frac{1}{16\pi^2}\left(\frac{9}{2}g_t^3\right) \quad , \quad \gamma_\phi = \frac{1}{64\pi^2}\left(12 g_t^2\right) .
\end{aligned} \tag{4}$$

and the anomalous dimension for the singlet field $\gamma_\varphi = 0$. Truncation of the effective potential at LL order requires counter terms corresponding to those in the Lagrangian

$$V_{eff} = V_{LL} + K_1\phi^4 + K_2\phi^2\varphi^2 + K_3\varphi^4 \tag{5}$$

where K_i are functions of the couplings. Defining $\rho^2 = \phi^2 + \varphi^2$ [24], the three renormalization conditions used to determine K_i

$$\left.\frac{d^4V_{eff}}{d\phi^4}\right|_{\rho=\mu} = \left.\frac{d^4V_{tree}}{d\phi^4}\right|_{\rho=\mu}, \quad \left.\frac{d^4V_{eff}}{d\varphi^4}\right|_{\rho=\mu} = \left.\frac{d^4V_{tree}}{d\varphi^4}\right|_{\rho=\mu} \tag{6}$$

$$\left.\frac{d^4V_{eff}}{d\phi^2 d\varphi^2}\right|_{\rho=\mu} = \left.\frac{d^4V_{tree}}{d\phi^2 d\varphi^2}\right|_{\rho=\mu} \tag{7}$$

are conveniently expressed as [15, 27, 28]

$$\left.\frac{d^4V_{eff}}{d\rho^4}\right|_{\rho=\mu} = \left.\frac{d^4V_{tree}}{d\rho^4}\right|_{\rho=\mu} \tag{8}$$

where V_{tree} is the tree level effective potential and a non-linear field parameterization is used with $\phi = n_\phi\rho$, $\varphi = n_\varphi\rho$, $n_\phi^2 + n_\varphi^2 = 1$.

To determine the couplings, we need to employ the vacuum expectation value (VEV) conditions which provides constraint for the minimum of the vacuum

$$\left.\frac{dV_{eff}}{d\phi}\right|_{\substack{\phi=v\\ \varphi=v_1}} = 0 \quad , \quad \left.\frac{dV_{eff}}{d\varphi}\right|_{\substack{\phi=v\\ \varphi=v_1}} = 0 . \tag{9}$$

where v is identified with the electroweak scale $v = 246.2\,\text{GeV}$ and $v_1 = 0$ corresponds to the unbroken case while $v_1 \neq 0$ for the broken case. In the unbroken case, we also identify the scale μ with the electroweak scale $\mu = v = 246.2$ to eliminate the higher-logarithmic terms. It should be noted that in the unbroken case, the above singlet VEV condition is trivial since it identically vanishes while this is not true in the broken case. The mass generated for the Higgs doublet M_H and singlet M_S are only dependent on the quadratic terms in the effective potential and can be determined from the eigenvalues of the mass matrix M

$$M = \left.\begin{pmatrix} \frac{dV_{eff}^2}{d\phi^2} & \frac{dV_{eff}^2}{d\phi d\varphi} \\ \frac{dV_{eff}^2}{d\varphi d\phi} & \frac{dV_{eff}^2}{d\varphi^2} \end{pmatrix}\right|_{\substack{\phi=v\\ \varphi=v_1}} \tag{10}$$

where in the unbroken case, the off-diagonal terms are zero and we obtain $M_H^2 = \left.\frac{dV_{eff}^2}{d\phi^2}\right|_{\substack{\phi=v\\ \varphi=v_1}}$, $M_S^2 = \left.\frac{dV_{eff}^2}{d\varphi^2}\right|_{\substack{\phi=v\\ \varphi=v_1}}$. Note that we have implicitly used the result that the effective potential kinetic term renormalization constant is unity in the CW scheme [15, 27].

In the unbroken symmetry case, Eq. (9) only contains one non-trivial constraint, and hence it is not possible to constrain all the couplings. We find that altering the singlet self-interaction coupling within the range $0 < \lambda_3 < 1$ only affects the physical dark matter mass predictions

less than 2.4%. We therefore typically set the dark matter self-interaction coupling to zero $\lambda_3 = 0$, corresponding to the case of weakly self-interacting dark matter, and comment on $\lambda_3 \neq 0$ as appropriate. The Higgs portal interaction λ_2 is then the only input parameter; it will be strongly constrained by dark matter abundance and direct detection experiments XENON100 [29] and LUX [30]. The Higgs mass prediction in this case is consistent with our previous findings and converges to approximately 125 GeV when higher loop contributions are included [18, 21].

We illustrate our predicted dark matter mass/coupling relation in the green curve in Fig. 1, which intersects the 10% (orange) and 100% (blue) dark matter abundance curves. These abundance curves are calculated using the results of Refs. [2, 31, 32]. Compared to the real scalar model [18], the complex singlet leads to a higher dark matter abundance because both components of the complex singlet contributes. Setting the dark matter self-interaction coupling to $\lambda_3 = 1$ shifts the results slightly from the green to the purple curve in the figure, retaining this qualitative feature. The shaded region in Fig. 1 represents the parameter space excluded by the LUX experiment at 95% CL [30], where we have used the most conservative effective Higgs-nucleon coupling [33] in the dark matter nucleon recoil cross section. Most of the parameter space below 85 GeV is ruled out by the LUX experiment [30], apart from a small region of parameter space in the $M_S \approx M_H/2$ resonant region, which is strongly constrained by the Higgs decay width [3, 34] (see Refs. [2, 35] for a comprehensive analysis). The contour of the LUX excluded region is approximated by a vertical line since the effective direct detection cross section has only a tiny logarithmic dependence on the coupling [35]. Combining the LUX [30] and dark matter abundance constraints, the complex singlet model admits a viable dark matter candidate $100\text{GeV} \leq \text{M}_\text{s} \leq 110\text{GeV}$ with Higgs portal interaction $0.05 \leq \lambda_2 \leq 0.2$ corresponding to $10\% - 100\%$ dark matter abundance. The viable dark matter candidates resulting from our analysis are very close to the boundary of the current direct detection experiments and will be in the detection region of the coming experiments XENON1T [36] and LUX 300 day results [30].

The broken-symmetry case $\langle S \rangle \neq 0$ is particularly interesting since the real component of the complex singlet will mix with the SM Higgs field, leading to one heavy and one light Higgs field, where the light state corresponds to the 125 GeV observed Higgs boson [22, 23]. In this situation dark matter is associated with an axion decoupled from the effective potential, which in turn does not provide dark matter phenomenological constraints on the coupling present in the unbroken case. Consequently the guiding principles used to extract a meaningful range of the free parameter space of (λ_2, λ_3) that remains after imposing Eqs. (9) are lost. To address this difficulty, we generalize our unbroken-symmetry methodology to incorporate a renormalization-scale optimization technique

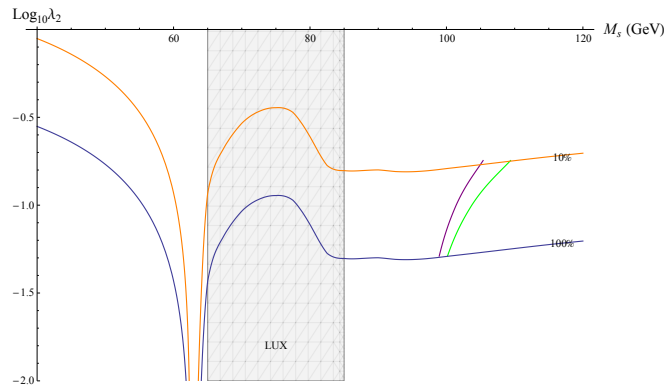

FIG. 1. Relationship between predicted dark matter mass and Higgs portal coupling λ_2 with $\lambda_3 = 0$ is shown by the green curve and $\lambda_3 = 1$ shown by purple curve along with various dark matter abundance curves 10% in yellow and 100% in blue to constrain the complex singlet model. The shaded region represents the parameter space which is excluded by the LUX experiment at 95% CL.

[25]. This technique was used to obtain an optimized renormalization scale in the MSSM with conventional symmetry breaking (CSB) [25], and is based on the idea that the complete effective potential should be scale independent. Since we do not have full information about the effective potential, which must be truncated at a particular loop order, the best that can be achieved is to find an optimized scale at which the scale-dependent minimum of the truncated effective potential self-consistently satisfies its RG equation.

It is nontrivial to generalize this optimization method to incorporate the radiative symmetry breaking (RSB) scenario. In the CSB scenario of the SM, all the couplings are known , and we only need to implement these known couplings as initial values and use the renormalization-group to run the couplings with the scale. The optimized scale is then explicitly determined by the point where the minimum of the effective potential satisfies its RG equation [25]. However, in the case of RSB, all the couplings are unknown and should be determined dynamically from the theory itself [15]. Without boundary values for the running couplings an intractable nonlinear numerical problem occurs in determining the optimized scale. To address this difficulty we define the scale-dependent minima $H_m(t)$ and $S_m(t)$ of the effective potential via

$$F\left(H_m(t), S_m(t), t, \lambda_i(t)\right) = \left.\frac{dV_{eff}}{dH}\right|_{\substack{H=H_m(t)\\ S=S_m(t)}} = 0\,, \quad (11)$$

$$G\left(H_m(t), S_m(t), t, \lambda_i(t)\right) = \left.\frac{dV_{eff}}{dS}\right|_{\substack{H=H_m(t)\\ S=S_m(t)}} = 0\,, \quad (12)$$

where $\mu = M_z \exp(t)$. We then differentiate these con-

straints with respect to t, and impose the condition [25]

$$\frac{dH_m(t*)}{dt} = -\gamma(t*)H_m(t*)\,, \quad \frac{dS_m(t*)}{dt} = 0 \tag{13}$$

for the optimized scale $t*$, resulting in the two constraints

$$0 = \frac{\partial F}{\partial t^*} - \gamma(t*)H_m(t^*)\frac{\partial F}{\partial H_m} + \beta_i(t^*)\frac{\partial F}{\partial \lambda_i}\,, \tag{14}$$

$$0 = \frac{\partial G}{\partial t^*} - \gamma(t*)H_m(t^*)\frac{\partial G}{\partial H_m} + \beta_i(t^*)\frac{\partial G}{\partial \lambda_i}\,. \tag{15}$$

Finally we connect the optimized minimum field configurations with the physical VEVs

$$H_m(t^*) = \langle H\rangle = v\,,\ S_m(t^*) = v_1\,. \tag{16}$$

Thus rather than requiring a global solution for $H_m(t)$ and $S_m(t)$ that is then used to determine t^* via (13), we have encoded the same information into the local constraints (14),(15) and the RG functions of the theory [26]. Note that the CW renormalization condition (8) is unaffected except for the replacement $\mu = M_Z \exp(t^*)$. It should be noted that in the case discussed in [25], only one optimization condition for the Higgs field is needed since they assumed supersymmetry is at a much higher scale and decoupled from the SM. We have generalized this optimization condition for both the Higgs and singlet fields, since the vacuum expectation value predicted here for the singlet may be near the electroweak scale, which cannot be decoupled. The above optimization conditions can be generalized further for more complicated models with multiple scalar fields.

We now have four constraints (9), (14), (15) for five parameters $\lambda_1(t^*), \lambda_2(t^*), \lambda_3(t^*), v_1, t^*$ where $\langle S\rangle = v_1$ is the VEV of the singlet field. If we additionally use the 125 GeV Higgs mass as an extra constraint, all five parameters in the model are determined. By using this method, we are able to find a solution for this model that provides a heavy Higgs at 554 GeV and a light Higgs at 125 GeV. The resulting parameters will be $\lambda_1(t^*) = 0.53$, $\lambda_3(t^*) = 1.926$, $\lambda_2(t^*) = -2.95$, $\langle S\rangle = 156\,\text{GeV}$, $\text{t}^* = -1.59$ respectively. The small scale $t^* = -1.59$ results from the scheme transformation $\mu_{CW} = \mu_{MS}/\lambda$, that is from the CW renormalization to the MS scheme [37, 38]. With the convention of the coupling we have chosen, the coupling solutions are normally larger than 1 and the scale in CW scheme is naturally smaller than the one in MS scheme i.e. $\mu_{CW} \leq \mu_{MS}$. We have also studied these couplings to assess their perturbative convergence using two loop RG functions [39]. We found $\beta_1^{2loop}/\beta_1^{1loop} = 5\times 10^{-5}$, $\beta_2^{2loop}/\beta_2^{1loop} = 0.04$, $\beta_3^{2loop}/\beta_3^{1loop} = 0.13$, which implies that higher-loop contributions are well-controlled. Numerically similar Higgs portal couplings in two doublet models were found in Ref. [14]. The mixing angle is strongly constrained by the LHC and electroweak precision measurements [40] where LHC Higgs signal rates provides the strongest constraint $\sin\theta \leq 0.5$ at around 500 GeV Higgs mass region. In our model, we find a mixing angle $\sin\theta = 0.467$, implying the above solution is not yet excluded and is in the LHC run 2 detection region. It should be noted that higher loop order effects might decrease the mixing angle further or alter the mass prediction of the heavier Higgs.

When the real component of the complex singlet obtains a VEV, the $U(1)$ global symmetry is spontaneously broken and generates a massless Goldstone boson containing the imaginary degree of freedom of the complex singlet. The complex singlet is conventionally written as $S(x) = \phi(x)\exp\left(\frac{ia(x)}{\sqrt{2}f_a}\right)$ where $a(x)$ is the axion field and f_a is the axion decay constant. Associating the $U(1)$ global symmetry with the Peccei-Quinn PQ symmetry [41, 42], the above Goldstone boson can be explained as the axion [43, 44] which addresses the dark matter problem. Normally, a large intermediate scale is required to connect to the large PQ symmetry breaking scale to address the smallness of the axion coupling. However, any intermediate scale between the EW scale and UV scale is not allowed in the CW mechanism [11, 45]. In [43, 44], the authors cleverly connect the smallness of the axion coupling to the lightness of the neutrino mass and generate an effective large f_a without introducing any large intermediate scale. Moreover, the $U(1)$ global symmetry considered in this work could also be made into a local symmetry, providing a new gauge interaction boson Z′; symmetry breaking at the TeV scale in this model was studied in Ref. [8].

It is interesting to analyze the underlying symmetry breaking mechanism for the broken case. We use the ratio of the tree-level VEV conditions as a measure of whether CSB or RSB is dominant. The ratio r is defined by

$$r = \left.\frac{dV_{tree}/d\phi^2}{dV_{tree}/d\varphi^2}\right|_{\substack{\phi=v\\ \varphi=v_1}} = \frac{2\lambda_1\left(\frac{v^2}{v_1^2}\right) + \lambda_2}{2\lambda_3 + \lambda_2\left(\frac{v^2}{v_1^2}\right)} \tag{17}$$

where $r \ll 1, r \gg 1, r \simeq 1$ correspond to CSB dominant in the Higgs sector, RSB dominant in the Higgs sector and the mixed scenario respectively. In the mixed scenario both CSB and RSB contribute to the EW symmetry breaking and we are not able to separate one from the other. Inputting the results $\lambda_1 = 0.53$, $\lambda_3 = 1.926, \lambda_2 = -2.95, \langle S\rangle = 156\,\text{GeV}$ of the broken case, we obtain $r = 0.1$ which implies conventional EW symmetry breaking in the Higgs sector triggered by the CW mechanism in the hidden sector. Note that the Higgs quartic coupling $\lambda_1 = 0.53$ obtained in our case is around four times larger than the SM one which is $\lambda_{\text{SM}} = 0.13$ implying large radiative corrections in the Higgs sector.

In summary, we have studied a conformally symmetric complex singlet extension of the SM with a Higgs portal interaction. Two different cases have been explored depending on whether the global $U(1)$ symmetry is spontaneously broken or unbroken. In the unbroken case, radiative EW symmetry breaking in the SM Higgs sector

is induced by CW mechanism [15]. In this case, the decay of the complex singlet is protected by the global $U(1)$ symmetry, which leads to an ideal dark matter candidate with around 100 GeV dark matter mass and significant proportion of the dark matter thermal relic abundance within the detection region of the up coming XENON1T [36] and LUX 300 day [30] experiments. In the broken case, we generalized our analysis by incorporating a modified version of the optimization method inspired by [25] and found the sequential symmetry breaking scenario, in which radiative symmetry breaking in the singlet sector triggers conventional EW symmetry breaking in the Higgs sector. We found there exists a second Higgs boson with an approximate 550 GeV mass and a mixing angle $\sin\theta \approx 0.47$, which satisfies the current experiment bound $\sin\theta \leq 0.5$ at around 500 GeV Higgs mass region provided by the LHC signal rates [40] that will be strengthened during LHC run 2.

T.G.S. and R.B.M are grateful for financial support from the Natural Sciences and Engineering Research Council of Canada (NSERC).

[1] V. Silveira, A. Zee, Phys. Lett. B 161 (1985) 136; J. McDonald, Phys. Rev. D 50 (1994) 3637; C.P. Burgess, M. Pospelov, T. ter Veldhuis, Nucl. Phys. B 619 (2001) 709; H. Davoudiasl, R. Kitano, T. Li, H. Murayama, Phys. Lett. B 609 (2005) 117; B. Patt, F. Wilczek, hep-ph/0605188; K. A. Meissner, H. Nicolai, Phys. Lett. B 648 (2007) 312.

[2] J. M. Cline and K. Kainulainen, JCAP **1301** (2013) 012.

[3] A. Djouadi, A. Falkowski, Y. Mambrini and J. Quevillon, Eur. Phys. J. C **73** (2013) 6, 2455.

[4] V. Barger, P. Langacker, M. McCaskey, M. Ramsey-Musolf and G. Shaughnessy, Phys. Rev. D **79** (2009) 015018

[5] M. Gonderinger, H. Lim and M. J. Ramsey-Musolf, Phys. Rev. D **86** (2012) 043511.

[6] R. Costa, A. P. Morais, M. O. P. Sampaio and R. Santos, Phys. Rev. D **92** (2015) 2, 025024.

[7] L. Basso, S. Moretti and G. M. Pruna, Phys. Rev. D **83** (2011) 055014.

[8] S. Iso and Y. Orikasa, PTEP **2013** (2013) 023B08.

[9] V. V. Khoze, C. McCabe and G. Ro, JHEP **1408** (2014) 026.

[10] L. Susskind, Phys. Rev. D 20 (1979) 2619.

[11] W. A. Bardeen, FERMILAB-CONF-95-391-T, 1995.

[12] G. 't Hooft, NATO Adv. Study Inst. Ser. B Phys. **59** (1980) 135.

[13] S. Weinberg, Phys. Lett. B **82** (1979) 387.

[14] C. T. Hill, Phys. Rev. D **89** (2014) 7, 073003.

[15] S. Coleman, E. Weinberg, Phys. Rev. D **7** (1973) 1888.

[16] R. Hempfling, Phys. Lett. B **379** (1996) 153; R. Foot, A. Kobakhidze, R. R. Volkas, Phys. Lett. B **655** (2007) 156; R. Foot, A. Kobakhidze, K. L. McDonald and R. R. Volkas, Phys. Rev. D **77** (2008) 035006; R. Foot, A. Kobakhidze and R. R. Volkas, Phys. Rev. D **82** (2010) 035005 C. Englert, J. Jaeckel, V. V. Khoze and M. Spannowsky, JHEP **1304** (2013) 060; V. V. Khoze and G. Ro, JHEP **1310** (2013) 075; W. -F. Chang, J. N. Ng and J. M. S. Wu, Phys. Rev. D **75** (2007) 115016; C. D. Carone, R. Ramos, Phys. Rev. D **88** (2013) 055020; L. Alexander-Nunneley and A. Pilaftsis, JHEP **1009** (2010) 021; A. Farzinnia, H. J. He and J. Ren, Phys. Lett. B **727** (2013) 141; K. Hashino, S. Kanemura and Y. Orikasa, arXiv:1508.03245 [hep-ph]; E. Gabrielli, M. Heikinheimo, K. Kannike, A. Racioppi, M. Raidal and C. Spethmann, Phys. Rev. D **89** (2014) 1, 015017.

[17] W. Altmannshofer, W. A. Bardeen, M. Bauer, M. Carena and J. D. Lykken, JHEP **1501** (2015) 032.

[18] T. G. Steele, Z. W. Wang, D. Contreras and R. B. Mann, Phys. Rev. Lett. **112** (2014) 17, 171602.

[19] V. Elias, R. B. Mann, D. G. C. McKeon and T. G. Steele, Phys. Rev. Lett. **91** (2003) 251601.

[20] V. Elias, R. B. Mann, D. G. C. McKeon and T. G. Steele, Nucl. Phys. B **678** (2004) 147; B **703** (2004) 413.

[21] T.G. Steele, Zhi-Wei Wang, Phys. Rev. Lett **110** (2013) 151601.

[22] ATLAS Collaboration, Phys. Lett. B **716** (2012) 1.

[23] CMS Collaboration, Phys. Lett. B **716** (2012) 30.

[24] E. Gildener, S. Weinberg, Phys. Rev. D **13** (1976) 3333.

[25] J. A. Casas, J. R. Espinosa, M. Quiros and A. Riotto, Nucl. Phys. B **436** (1995) 3 [Nucl. Phys. B **439** (1995) 466].

[26] J. Elias-Miro, J. R. Espinosa, G. F. Giudice, H. M. Lee and A. Strumia, JHEP **1206** (2012) 031.

[27] R. Jackiw, Phys. Rev. D **9** (1974) 1686.

[28] K. Inoue, A. Kakuto and Y. Nakano, Prog. Theor. Phys. 63 (1980) 234.

[29] E. Aprile *et al.* [XENON100 Collaboration], Phys. Rev. Lett. **109** (2012) 181301.

[30] D. S. Akerib *et al.* [LUX Collaboration], Phys. Rev. Lett. **112** (2014) 091303.

[31] G. Steigman, B. Dasgupta and J. F. Beacom, Phys. Rev. D **86** (2012) 023506

[32] S. Dittmaier *et al.*, arXiv:1101.0593.

[33] F. S. Sage and R. Dick, Astropart. Phys. **71** (2015) 31

[34] A. Djouadi, O. Lebedev, Y. Mambrini and J. Quevillon, Phys. Lett. B **709** (2012) 65.

[35] J. M. Cline, K. Kainulainen, P. Scott and C. Weniger, Phys. Rev. D **88** (2013) 055025.

[36] E. Aprile [XENON1T Collaboration], arXiv:1206.6288.

[37] T. G. Steele, Z. W. Wang and D. G. C. McKeon, Phys. Rev. D **90** (2014) 10, 105012

[38] C. Ford and D. R. T. Jones, Phys. Lett. B **274** (1992) 409 [Phys. Lett. B **285** (1992) 399].

[39] G. Ballesteros and C. Tamarit, JHEP09(2015)210.

[40] T. Robens and T. Stefaniak, Eur. Phys. J. C **75** (2015) 3, 104.

[41] R. D. Peccei and H. R. Quinn, Phys. Rev. Lett. **38** (1977) 1440.

[42] S. Weinberg, Phys. Rev. Lett. **40** (1978) 223.

[43] K. A. Meissner and H. Nicolai, Eur. Phys. J. C **57** (2008) 493.

[44] A. Latosinski, K. A. Meissner and H. Nicolai, arXiv:1010.5417 [hep-ph].

[45] M. Shaposhnikov, arXiv:0708.3550 [hep-th].